

Two-parameter bifurcations analysis of a delayed high-temperature superconducting maglev model with guidance force

Cite as: Chaos **32**, 083128 (2022); <https://doi.org/10.1063/5.0104854>

Submitted: 21 June 2022 • Accepted: 25 July 2022 • Published Online: 16 August 2022

 Qinrui Dai



[View Online](#)



[Export Citation](#)



[CrossMark](#)

APL Machine Learning

Open, quality research for the networking communities

Now Open for Submissions

[LEARN MORE](#)

Two-parameter bifurcations analysis of a delayed high-temperature superconducting maglev model with guidance force

Cite as: Chaos 32, 083128 (2022); doi: 10.1063/5.0104854

Submitted: 21 June 2022 · Accepted: 25 July 2022 ·

Published Online: 16 August 2022



View Online



Export Citation



CrossMark

Qinrui Dai^{a)} 

AFFILIATIONS

School of Mathematics and Statistics, Wuhan University, Wuhan 430072, China

^{a)}Author to whom correspondence should be addressed: dqrhit@qq.com

ABSTRACT

A modified high-temperature superconducting maglev model is studied in this paper, mainly considering the influence of time delay on the dynamic properties of the system. For the original model without time delay, there are periodic equilibrium points. We investigate its stability and Hopf bifurcation and study the bifurcation properties by using the center manifold theorem and the normal form theory. For the delayed model, we mainly study the co-dimension two bifurcations (Bautin and Hopf-Hopf bifurcations) of the system. Specifically, we prove the existence of Bautin bifurcation and calculate the normal form of Hopf-Hopf bifurcation through the bifurcation theory of functional differential equations. Finally, we numerically simulate the abundant dynamic phenomena of the system. The two-parameter bifurcation diagram in the delayed model is given directly. Based on this, some nontrivial phenomena of the system, such as periodic coexistence and multistability, are well presented. Compared with the original ordinary differential equation system, the introduction of time delay makes the system appear chaotic behavior, and with the increase in delay, the variation law between displacement and velocity becomes more complex, which provides further insights into the dynamics of the high-temperature superconducting maglev model.

Published under an exclusive license by AIP Publishing. <https://doi.org/10.1063/5.0104854>

Bifurcations, especially co-dimension two bifurcations, are very common in nonlinear dynamical systems. The periodic coexistence, multistability, and chaos associated with co-dimension two bifurcations are of great significance to the study of the dynamic behavior of the system. The high-temperature superconducting (HTS) maglev model is a typical nonlinear system, but its bifurcation research is not sufficient, and some internal dynamic behaviors have not been mined. Therefore, this paper studies a delayed high-temperature superconducting maglev model from the perspective of co-dimension two bifurcations. Moreover, some nontrivial phenomena are simulated and theoretical explanations are given.

I. INTRODUCTION

Magnetic levitation can be realized by using the diamagnetism of superconductors. Recently, high-temperature superconducting (HTS) maglev technology has been developed rapidly and applied in high-speed railways, which has also attracted the attention of many

researchers.^{1–4} Compared with the previous railway, subway, and light rail, the HTS maglev system has great advantages, such as high speed, low noise, and self-stability. However, due to its low damping, the system is easily disturbed by cross wind, irregular track, train crossing, and other external environments, which leads to a long response time and weak anti-interference ability.⁵ Therefore, it is necessary to study the dynamics of the HTS maglev system. To date, many scholars measure the magnetic levitation force, stiffness of levitation force, and force relaxation time of the system by simulating the HTS maglev environment.^{6–8} At the same time, some papers have established mathematical models to study the dynamic properties of the HTS maglev system. For example, a mathematical model of the superconducting flywheel energy storage system with radial high-temperature superconducting bearing is established in Ref. 9, and the electromagnetic characteristics of HTS bearing in the suspension process are studied by the finite element method (FEM). Li *et al.*¹⁰ used the German low interference track spectrum as the irregularity of permanent magnet guideway, then established the mathematical model of an HTS maglev vehicle with an active driver, and simulated the dynamic response of the system. In Ref. 11,

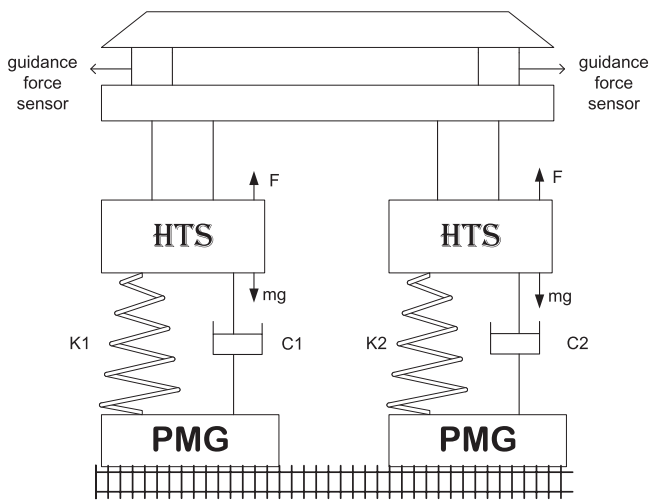


FIG. 1. Schematic diagrams of the simplified HTS magnetic dynamical system with a guidance force sensor.

a two-dimensional coupling model is proposed to fit the experimental data, and the dynamic characteristics of the HTS maglev system in two-dimensional space are studied. In Ref. 12, the electromagnetic thermal multi-physical coupling model is established and its dynamic characteristics are analyzed, especially the suspension height drift of HTS bulk above the permanent magnet guide rail. Some articles established HTS systems derived from critical state, elliptical models, or power-law models and carried out some numerical simulations.^{13–16} Levitation force and guidance force are very important to the dynamic analysis of the HTS system,^{17–19} but there are few reports on the guidance force model. Some researchers^{14,20} believe that the guidance force depends not only on the relative displacement but also on the velocity of the relative motion, which determines the change of the external field, resulting in the shielding current induced in the bulk superconductor during the relative motion. Therefore, considering the guidance force, the authors in Ref. 20 deduced and established the following two-dimensional ordinary differential model:

$$\begin{cases} \frac{dy_1}{dt} = y_2, \\ \frac{dy_2}{dt} = \frac{\alpha \sin(\beta y_1) + \eta_1 y_2 + \eta_2 y_2^3}{m}, \end{cases} \quad (1)$$

where t is the time, y_1 and y_2 represent the displacement and velocity of the vehicle at time t , respectively. The parameters α and β stand for the maximum guidance force and the wavelength of the guidance force, respectively. η_1 and η_2 denote the linear and nonlinear coefficients of damping, respectively. A simplified HTS guidance force dynamical system with two degrees-of-freedom is shown in Fig. 1. Equation (1) is somewhat similar to the classical simple pendulum equation. In fact, when parameter $\eta_2 = 0$, Eq. (1) becomes a simple pendulum equation considering friction resistance and without torque.

For the nonlinear guidance force hysteretic model, the time delay can usually be considered (see Refs. 21–23 for details). Taking into account the delay τ of the linear part of the velocity, we can obtain the following functional differential equation:

$$\begin{cases} \frac{dy_1}{dt} = y_2, \\ \frac{dy_2}{dt} = \frac{\alpha \sin(\beta y_1) + \eta_1 y_2(t-\tau) + \eta_2 y_2^3}{m}. \end{cases} \quad (2)$$

These papers above only carry out numerical analysis or stability analysis of the proposed mathematical models but rarely involve more complex dynamic property analysis, such as bifurcation, multistability, periodic coexistence, and so on. For nonlinear systems, bifurcation phenomena, especially co-dimension two bifurcations, are very common, which is important to study the dynamic properties of the system.

Inspired by the above analysis, this paper mainly studies system (1) and its delay system (2) from the perspective of bifurcation. Therefore, the rest of this paper is organized as follows: Sec. II gives some preliminary notes. In Sec. III, we analyze the stability and Hopf bifurcation of system (1). Co-dimension two bifurcations of system (2) are investigated in Sec. IV and in Sec. V. Specifically, we investigate the co-dimension two: Bautin bifurcation and Hopf–Hopf bifurcation and the normal form of bifurcations are given by the center manifold theorem and the normal form theory of functional differential equation. In order to support our theoretical analysis, in Sec. VI, we simulate the Hopf bifurcation occurred in system (1). For system (2), we draw a two-parameter bifurcation diagram with τ and η_1 as bifurcation parameters and divide the bifurcation diagram into different regions according to different bifurcation curves, and the key regions are also numerically simulated. Finally, Sec. VII is a brief conclusion and discussion section.

II. PRELIMINARIES

Consider a general continuous-time dynamical system with parameters $\gamma \in \mathbb{R}^r$, defined by

$$\dot{x} = f(x, \gamma), \quad (3)$$

where $x \in \mathbb{R}^n$, f is sufficiently smooth with $f(0) = 0$. Define $\lambda_1, \lambda_2, \dots, \lambda_k$ as the eigenvalues of the Jacobian matrix A evaluated at the equilibrium point $x_0 = 0$. Given that there are k_- eigenvalues (counting multiplicities) with $\text{Re } \lambda < 0$, k_0 eigenvalues with $\text{Re } \lambda = 0$ and k_+ eigenvalues with $\text{Re } \lambda > 0$, respectively. T^x stands for the generalized linear eigenspace of matrix A corresponding to the union of the k_0 eigenvalues on the imaginary axis.

Theorem 1 (Center manifold theorem²⁴). *There is a locally defined smooth k_0 -dimensional invariant manifold $W_{loc}^c(0)$ of (3), which is tangent to T^x at $x = 0$. Moreover, for all $t \geq 0$ ($t \leq 0$), there is a neighborhood U of $x = 0$ such that if $\varphi^t x \in U$, then $\varphi^t x \rightarrow W_{loc}^c(0)$ when $t \rightarrow +\infty$ ($t \rightarrow -\infty$).*

Definition 1 (Ref. 24). *The manifold $W_{loc}^c(0)$ is called the center manifold.*

Construct a simple system

$$\dot{\vartheta} = s(\vartheta, v; \sigma), \quad (4)$$

where $\vartheta \in \mathbb{R}^n, v \in \mathbb{R}^r, \sigma \in \mathbb{R}^l$, and for $v = 0$, there is an equilibrium $\vartheta = 0$ satisfying r bifurcation conditions determining a Co-dim r bifurcation of this equilibrium. σ is a vector composed of coefficients $\sigma_i (i = 1, \dots, l)$.

Definition 2 (Topological normal form²⁴). System (4) is called a topological normal form for the bifurcation if any generic system (3) with the equilibrium $x = 0$ satisfying the same bifurcation conditions at $\gamma = 0$ is locally topologically equivalent near the origin to (4) for some values of the coefficients σ_i .

For $\gamma \in \mathbb{R}^2$, assume that Jacobian matrix A has a pair of conjugate complex roots $\lambda_{1,2}(\gamma) = \mu(\gamma) \pm i\omega(\gamma)$ for all sufficiently small $|\gamma|$. The following three conditions are known as the genericity conditions for Bautin bifurcation:

(H1) $l_1(\gamma)$ is the first Lyapunov coefficient with $l_1(0) = 0$.

(H2) The second Lyapunov coefficient $l_2(0) \neq 0$.

(H3) The map $\varphi : (\gamma_1, \gamma_2) \mapsto (\mu(\gamma), l_1(\gamma))$ is regular at $\gamma = 0$.

Theorem 2 (Ref. 24). Suppose (H1)–(H3) hold, then system (3) undergoes a Bautin bifurcation, and this system is locally topologically equivalent near the origin to the following complex normal form:

$$\dot{z} = (v_1 + i)z + v_2 z|z|^2 + \text{sign}(l_2(0))z|z|^4.$$

The infinitesimal generator has at least two pairs of purely imaginary eigenvalues, which is a necessary condition for the Hopf–Hopf bifurcation of the system. The main dynamic feature of Hopf–Hopf bifurcation is the occurrence of an invariant 3-torus. For the normal form and a detailed discussion for a delayed system at the nonresonant Hopf–Hopf bifurcation point, the reader is referred to Refs. 25 and 26.

III. STABILITY AND HOPF BIFURCATION OF SYSTEM (1)

For system (1), any equilibrium point $E_n(y_{n1}, y_{n2})$ satisfies the following equation:

$$\begin{cases} y_{n2} = 0, \\ \alpha \sin(\beta y_{n1}) + \eta_1 y_{n2} + \eta_2 y_{n2}^3 = 0. \end{cases} \quad (5)$$

Solving Eq. (5) is easy to obtain $E_n(y_{n1}, y_{n2}) = E_n\left(\frac{n\pi}{\beta}, 0\right)$, where $n \in \mathbb{Z}$. From the physical description of the system, it is obvious that model (1) has only two equilibrium points, corresponding to $E_0(0, 0)$ and $E_1\left(\frac{\pi}{\beta}, 0\right)$, respectively, and other equilibrium points coincide with these two equilibrium points. However, in the process of qualitative analysis, we played down this problem and retained all the equilibrium points. Thus, the Jacobian matrix of system (1) at equilibrium point $E_n\left(\frac{n\pi}{\beta}, 0\right)$ is

$$J_{E_n} = \begin{pmatrix} 0 & 1 \\ \frac{\beta\alpha}{m} \cos(n\pi) & \frac{\eta_1}{m} \end{pmatrix},$$

and the characteristic equation is easily reduced to

$$\lambda^2 - \frac{\eta_1}{m}\lambda - \frac{\beta\alpha}{m} = 0, \quad (6)$$

when n is even, or

$$\lambda^2 - \frac{\eta_1}{m}\lambda + \frac{\beta\alpha}{m} = 0, \quad (7)$$

when n is odd. For the convenience of later description, here we record these two kinds of equilibrium points as “even equilibrium points” and “odd equilibrium points,” respectively. Therefore, following from the Routh–Hurwitz criteria, the stability of equilibrium point $E_n\left(\frac{n\pi}{\beta}, 0\right)$ is summarized in Theorem 3.

Theorem 3. If $\frac{\beta\alpha}{m} < 0$ ($\frac{\beta\alpha}{m} > 0$), $\frac{\eta_1}{m} < 0$ and n is even (odd), then the equilibrium point $E_n\left(\frac{n\pi}{\beta}, 0\right)$ is locally asymptotically stable.

From Theorem 3, we can know that the stability of odd and even equilibrium points is always the opposite, that is, one is stable and the other is unstable. Therefore, without loss of generality, we only discuss the Hopf bifurcation of the system at zero equilibrium point $E_0(0, 0)$. If $\eta_1 = 0$ and $\frac{\beta\alpha}{m} > 0$, then the characteristic equation (6) has a pair of pure imaginary roots $\lambda_{1,2} = \pm i\sqrt{\frac{\beta\alpha}{m}}$. In this case, if the transversality condition is satisfied, theoretically, Hopf bifurcation occurs in the system. To this end, deriving both sides of Eq. (6) with respect to η_1 yields $2\lambda \frac{d\lambda}{d\eta_1} - \frac{1}{m}\lambda - \frac{\eta_1}{m} \frac{d\lambda}{d\eta_1} = 0$. Then,

$$\frac{d\lambda}{d\eta_1} = \frac{\frac{1}{m}\lambda}{2\lambda - \frac{\eta_1}{m}} = \frac{\frac{1}{m}i\sqrt{\frac{\beta\alpha}{m}}}{2i\sqrt{\frac{\beta\alpha}{m}} - \frac{\eta_1}{m}} = \frac{-\frac{2}{m}\frac{\beta\alpha}{m} + i\frac{1}{m}\sqrt{\frac{\beta\alpha}{m}}\frac{\eta_1}{m}}{-4\frac{\beta\alpha}{m} - \frac{\eta_1^2}{m^2}},$$

so $\text{Re}\left(\frac{d\lambda}{d\eta_1}\right)_{\eta_1=0} = \frac{1}{2m} > 0$. To study the properties of Hopf bifurcation, the normal form and the first Lyapunov coefficient of system (1) are calculated. For convenience, write system (1) as

$$\begin{pmatrix} \frac{dy_1}{dt} \\ \frac{dy_2}{dt} \end{pmatrix} = \begin{pmatrix} 0 & 1 \\ \frac{\alpha\beta}{m} & \frac{\eta_1}{m} \end{pmatrix} \begin{pmatrix} y_1 \\ y_2 \end{pmatrix} + \begin{pmatrix} 0 \\ f(y_1, y_2, \eta_1) \end{pmatrix}, \quad (8)$$

where $f(y_1, y_2, \eta_1) = -\frac{1}{6}\beta^3 y_1^3 + \frac{\eta_2}{m}y_2^2 + h.o.t.$ Introduce a matrix

$$T = \begin{pmatrix} T_1 & T_2 \\ 1 & 0 \end{pmatrix},$$

where $T_1 = -\frac{\eta_1}{2\alpha\beta}$ and $T_2 = -\frac{\sqrt{-4m\alpha\beta-\eta_1^2}}{2\alpha\beta}$. Therefore, the inverse matrix of T is

$$T^{-1} = \begin{pmatrix} 0 & 1 \\ \frac{1}{T_2} & -\frac{T_1}{T_2} \end{pmatrix}.$$

Apparently,

$$T_{10} = T_1|_{\eta_1^*=0} = 0, T_{20} = T_2|_{\eta_1^*=0} = -\frac{\sqrt{-m\alpha\beta}}{\alpha\beta}.$$

By a linear transformation $\begin{pmatrix} y_1 \\ y_2 \end{pmatrix} = T \begin{pmatrix} x \\ y \end{pmatrix}$, system (8) can be transformed into

$$\begin{pmatrix} \frac{dx}{dt} \\ \frac{dy}{dt} \end{pmatrix} = \begin{pmatrix} \xi(\eta_1) & -\omega(\eta_1) \\ \omega(\eta_1) & \xi(\eta_1) \end{pmatrix} \begin{pmatrix} x \\ y \end{pmatrix} + \begin{pmatrix} f(x, y, \eta_1) \\ g^1(x, y, \eta_1) \end{pmatrix}, \quad (9)$$

where

$$\xi(\eta_1) = \frac{\eta_1}{2m}, \quad \omega(\eta_1) = \frac{\sqrt{-4m\alpha\beta-\eta_1^2}}{2m},$$

and

$$\begin{aligned} f^1(x, y, \eta_1) &= \left(-\frac{1}{6}\beta^3 T_1^2 + \frac{\eta_2}{m} \right) x^3 - \frac{1}{2}\beta^3 T_1^2 T_2 x^2 y \\ &\quad - \frac{1}{2}\beta^3 T_1 T_2^2 x y^2 - \frac{1}{6}\beta^3 T_2^2 y^3, \\ g^1(x, y, \eta_1) &= -\frac{T_1}{T_2} f^1(x, y). \end{aligned}$$

In polar coordinates, the normal form of system (9) is

$$\begin{cases} \dot{\rho} = \xi(\eta_1) + a(\eta_1)\rho^3 + h.o.t., \\ \dot{\theta} = \omega(\eta_1) + c(\eta_1)\rho^2 + h.o.t. \end{cases}$$

The stability of the periodic solution bifurcating from E_0 is determined by the sign of $a(\eta_1^*)$. Thus, substituting T_{10}, T_{20} and $x = x_0 = 0, y = y_0 = 0$ into

$$\begin{aligned} a(\eta_1^*) &= \frac{1}{16} \left(f_{xxx}^1 + f_{xyy}^1 + g_{xxy}^1 + g_{yyy}^1 \right) \\ &\quad + \frac{1}{16\omega(\eta_1^*)} \left[f_{xy}^1 (f_{xx}^1 + f_{yy}^1) - g_{xy}^1 (g_{xx}^1 + g_{yy}^1) - g_{xx}^1 g_{xx}^1 + f_{yy}^1 g_{yy}^1 \right], \end{aligned}$$

directly, the calculation can obtain $a(\eta_1^*) = \frac{\eta_2}{16m}$. Referring to Ref. 24, the first Lyapunov coefficient is

$$l_1(0) = \frac{a(\eta_1^*)}{\omega(\eta_1^*)} = \frac{\eta_2}{16\sqrt{-m\alpha\beta}}.$$

Therefore, the existence and properties of Hopf bifurcation can be summarized as follows:

Theorem 4. Hopf bifurcation occurs in system (1) at equilibrium point $E_0(0, 0)$ when $\eta_1 = 0$ and $\frac{\beta\alpha}{m} < 0$. If $l_1(0) < 0$ ($l_1(0) > 0$), then the bifurcation is supercritical (subcritical), and there is a stable (unstable) periodic solution bifurcating from E_0 .

Remark 1. Similarly, the conditions of the Hopf bifurcation at other even equilibriums of the system are the same as those at zero equilibriums, that is, when the conditions in Theorem 4 are met, all even equilibriums occur Hopf bifurcation, while odd equilibriums become unstable saddle points. On the contrary, when $\eta_1 = 0$ and $\frac{\beta\alpha}{m} > 0$, the stability of odd and even equilibriums is interchanged.

IV. BAUTIN BIFURCATION IN SYSTEM (2)

In this section, we analyze the bifurcation of delayed system (2) at zero equilibrium E_0 . The linearized system at zero equilibrium is given by

$$\begin{pmatrix} \frac{dy_1}{dt} \\ \frac{dy_2}{dt} \end{pmatrix} = \begin{pmatrix} 0 & 1 \\ \frac{\alpha\beta}{m} & 0 \end{pmatrix} \begin{pmatrix} y_1 \\ y_2 \end{pmatrix} + \begin{pmatrix} 0 & 0 \\ 0 & \frac{\eta_1}{m} \end{pmatrix} \begin{pmatrix} y_1(t-\tau) \\ y_2(t-\tau) \end{pmatrix}. \quad (10)$$

The characteristic equation of (10) is

$$\lambda^2 - \frac{\eta_1}{m} e^{-\lambda\tau} \lambda - \frac{\alpha\beta}{m} = 0. \quad (11)$$

Let $\lambda = i\omega$ be a root of (11) and substitute it into (11),

$$-\omega^2 - \frac{\eta_1}{m} e^{-i\omega\tau} (i\omega) - \frac{\alpha\beta}{m} = 0. \quad (12)$$

Separating real and imaginary parts of Eq. (12), we have

$$\begin{cases} -\frac{\alpha\beta}{m} - \omega^2 = \frac{\eta_1}{m} \omega \sin(\tau\omega), \\ -\frac{\eta_1}{m} \omega \cos(\tau\omega) = 0. \end{cases} \quad (13)$$

Clearly,

$$\omega^4 + \left(2\frac{\alpha\beta}{m} - \frac{\eta_1^2}{m^2} \right) \omega^2 + \frac{\alpha^2\beta^2}{m^2} = 0. \quad (14)$$

Set $u = \omega^2$. Equation (14) is equivalent to

$$u^2 + \left(2\frac{\alpha\beta}{m} - \frac{\eta_1^2}{m^2} \right) u + \frac{\alpha^2\beta^2}{m^2} = 0. \quad (15)$$

Define here

$$w(u) = u^2 + \left(2\frac{\alpha\beta}{m} - \frac{\eta_1^2}{m^2} \right) u + \frac{\alpha^2\beta^2}{m^2}. \quad (16)$$

For (15), we have

Lemma 1. If $\Delta > 0$ and $\frac{2\alpha\beta}{m} - \frac{\eta_1^2}{m^2} < 0$, then Eq. (15) has two different positive roots u_1 and u_2 . Accordingly, Eq. (14) consists of two positive roots $\omega_k = \sqrt{u_k}, k = 1, 2$, where $u_1 = \frac{-2m\alpha\beta + \eta_1^2 - m^2\sqrt{\Delta}}{2m^2}$, $u_2 = \frac{-2m\alpha\beta + \eta_1^2 + m^2\sqrt{\Delta}}{2m^2}$ and $\Delta = \left(\frac{2\alpha\beta}{m} - \frac{\eta_1^2}{m^2} \right)^2 - \frac{4\alpha^2\beta^2}{m^2}$.

Then, from Eq. (13), the critical value of τ for Hopf bifurcation is

$$\tau_k^j = \begin{cases} \frac{1}{\omega_k} \left(\frac{\pi}{2} + 2j\pi \right) & \text{if } \sin(\tau\omega) > 0, \\ \frac{1}{\omega_k} \left(\frac{3\pi}{2} + 2j\pi \right) & \text{if } \sin(\tau\omega) < 0, \end{cases} \quad j = 0, 1, 2, \dots, k = 1, 2,$$

and $\pm i\omega_k$ is a pair of pure imaginary roots of Eq. (11) when $\tau = \tau_k^j, j = 0, 1, 2, \dots, k = 1, 2$. Define $\tau_0 = \min_{k=1,2} \{\tau_k^0\}$, $\omega_0 = \omega_k$. Let $\lambda(\tau) = \varphi(\tau) + i\gamma(\tau)$ be the root of Eq. (11) and satisfy $\varphi(\tau_0) = 0$, $\gamma(\tau_0) = \omega_0$. Differentiating both sides of (11) with respect to τ leads to

$$2\lambda \frac{d\lambda}{d\tau} + \frac{\eta_1}{m} \lambda \tau e^{-\lambda\tau} \frac{d\lambda}{d\tau} + \frac{\eta_1}{m} \lambda^2 e^{-\lambda\tau} - \frac{\eta_1}{m} e^{-\lambda\tau} \frac{d\lambda}{d\tau} = 0.$$

Further,

$$\frac{d\lambda}{d\tau} = -\frac{\frac{\eta_1}{m} \lambda^2 e^{-\lambda\tau}}{2\lambda + \frac{\eta_1}{m} \tau \lambda e^{-\lambda\tau} - \frac{\eta_1}{m} e^{-\lambda\tau}}$$

and

$$\left(\frac{d\lambda}{d\tau} \right)^{-1} = -\frac{2\lambda e^{\lambda\tau} - \frac{\eta_1}{m}}{\frac{\eta_1}{m} \lambda^2} - \frac{\tau}{\lambda}. \quad (17)$$

Hence, substituting $\lambda = i\omega_0$ into (17) yields

$$\begin{aligned} \text{sign}\left[\frac{d(\text{Re } \lambda)}{d\tau}\right]_{\tau=\tau_k} &= \text{sign}\left[\text{Re}\left(\frac{d\lambda}{d\tau}\right)^{-1}\right]_{\tau=\tau_k} \\ &= \text{sign}\left[\text{Re}\left(-\frac{2\lambda e^{\lambda\tau} - \frac{\eta_1}{m}}{\frac{\eta_1}{m}\lambda^2} - \frac{\tau}{\lambda}\right)\right] \\ &= \text{sign}\left(\frac{\frac{2\alpha\beta}{\eta_1} + \frac{2m\omega_0^2}{\eta_1} - \frac{\eta_1}{m}}{\frac{\eta_1}{m}\omega_0^2}\right) \\ &= \text{sign}\left(\frac{\eta_1 w'(u)}{m\omega_0^2}\right) > 0. \end{aligned}$$

So far, all the conditions for the Hopf bifurcation of delayed system (2) have been satisfied. Thus, we have the following theorem:

Theorem 5. Zero equilibrium E_0 is locally asymptotically stable (unstable) when $\tau \in (0, \tau_0)$ ($\tau > \tau_0$), and Hopf bifurcation occurs in system (2) at zero equilibrium E_0 when $\tau = \tau_0$.

Now, the properties of Hopf bifurcation can be obtained from some standard theories. By scaling $t \rightarrow \frac{t}{\tau}$ and perturbing $\mu = \tau - \bar{\tau}$, $\varsigma = \eta_1 - \bar{\eta}_1$, system (2) is equivalent to the following functional differential equation in phase space $C = C([-1, 0], \mathbb{R}^2)$:

$$\dot{u}(t) = L(\mu, \varsigma)u_t + F(\mu, \varsigma, u_t), \quad (18)$$

where $u(t) = (y_1(t), y_2(t))^T \in \mathbb{R}^2$, $L : C \rightarrow \mathbb{R}^2$, $u_t = u(t + \theta)$, $\theta \in [-1, 0]$ and $F : \mathbb{R}^2 \times C \rightarrow \mathbb{R}^2$. For $\phi = (\phi_1, \phi_2) \in C$, we have

$$\begin{aligned} L(\mu, \varsigma)\phi &= (\bar{\tau} + \mu) \begin{pmatrix} 0 & 1 \\ \frac{\alpha\beta}{m} & 0 \end{pmatrix} \begin{pmatrix} \phi_1(0) \\ \phi_2(0) \end{pmatrix} \\ &\quad + (\bar{\tau} + \mu) \begin{pmatrix} 0 & 0 \\ 0 & \bar{\eta}_1 + \varsigma \end{pmatrix} \begin{pmatrix} \phi_1(-1) \\ \phi_2(-1) \end{pmatrix} \end{aligned}$$

and

$$F(\mu, \varsigma, \phi) = (\bar{\tau} + \mu) \begin{pmatrix} F_{11} \\ F_{12} \end{pmatrix},$$

where

$$F_{11} = 0,$$

$$F_{12} = -\frac{1}{6}\beta^3\phi_1^3(0) + \frac{\eta_2}{m}\phi_2^3(0).$$

By the Riesz representation theorem, there exists a matrix that is a bounded variation function $\eta(\theta, \mu, \varsigma)$ for $\theta \in [-1, 0]$ such that

$$L(\mu, \varsigma)\varphi = \int_{-1}^0 d\eta(\theta, \mu, \varsigma)\varphi(\theta), \text{ for } \varphi \in C[-1, 0].$$

The Dirac function δ can actually be selected for $\eta(\theta, \mu, \varsigma)$,

$$\begin{aligned} \eta(\theta, \mu, \varsigma) &= (\bar{\tau} + \mu) \begin{pmatrix} 0 & 1 \\ \frac{\alpha\beta}{m} & 0 \end{pmatrix} \delta(\theta) \\ &\quad + (\bar{\tau} + \mu) \begin{pmatrix} 0 & 0 \\ 0 & \bar{\eta}_1 + \varsigma \end{pmatrix} \delta(\theta + 1). \end{aligned}$$

Now, define the operator as

$$A(\mu, \varsigma)\phi = \begin{cases} \frac{d\phi(\theta)}{d\theta} & \text{for } \theta \in [-1, 0], \\ \int_{-1}^0 d\eta(\theta, \mu, \varsigma)\phi(\theta) & \text{for } \theta = 0 \end{cases}$$

and

$$R(\mu, \varsigma)\phi = \begin{cases} 0 & \text{for } \theta \in [-1, 0], \\ F(\mu, \varsigma, \theta) & \text{for } \theta = 0. \end{cases}$$

System (18) can be further transformed into the following form:

$$\dot{u}_t = A(\mu, \varsigma)u_t + R(\mu, \varsigma)u_t,$$

where still $u_t = u(t + \theta)$, $\theta \in [-1, 0]$. In the following, we need to define an inner product and the adjoint operator of A to describe the center manifold near $(\mu, \varsigma) = (0, 0)$. For $\psi \in C^* = C([-1, 0], (R^2)^*)$, denote the adjoint operator,

$$A^*(\mu, \varsigma)\psi = \begin{cases} -\frac{d\psi(s)}{ds} & \text{for } s \in (0, 1], \\ \int_{-1}^0 d\eta^T(\xi, 0, 0)\psi(-\xi) & \text{for } s=0, \end{cases}$$

where η^T is the transpose matrix of η , and for $\phi \in C[-1, 0]$, $\psi \in C[0, 1]$, the bilinear form

$$\langle \psi(s), \phi(\theta) \rangle = \bar{\psi}(0)\phi(0) - \int_{-1}^0 \int_0^\theta \bar{\psi}(\xi - \theta)d\eta(\theta, 0, 0)\phi(\xi)d\xi, \quad (19)$$

satisfying $\langle \psi, A\phi \rangle = \langle A^*\psi, \phi \rangle$. To obtain the properties of the Hopf bifurcation, we need to calculate the eigenvector of the eigenvalue $\pm i\bar{\tau}\omega_0$ of Eq. (11), so we have

Lemma 2. $q(\theta) = (1, q_1)^T e^{i\bar{\tau}\omega_0\theta}$ is the eigenvector of A corresponding to $i\bar{\tau}\omega_0$, and $q^*(s) = D(1, q_1^*)^T e^{i\bar{\tau}\omega_0 s}$ is the eigenvector of A^* corresponding to $-i\bar{\tau}\omega_0$, meeting the requirements $\langle q^*(s), q(\theta) \rangle = 1$, $\langle q^*(s), \bar{q}(\theta) \rangle = 0$, where $q_1 = i\omega_0$, $q_1^* = -\frac{\alpha\beta}{m(i\omega_0 + \bar{\eta}_1 e^{-i\omega_0})}$, and $\bar{D} = \frac{1}{1 + q_1 \bar{q}_1^* - \bar{\tau} \bar{\eta}_1 q_1 e^{-i\bar{\tau}\omega_0}}$.

Proof. Letting $q(\theta)$ be the eigenvector of $i\bar{\tau}\omega_0$, we have

$$Aq(\theta) = \frac{dq(\theta)}{d\theta} = i\bar{\tau}\omega_0 q(\theta), \theta \in [-1, 0].$$

Solving the above differential equation, it is easy to know that $q(\theta)$ has the following form:

$$q(\theta) = (1, q_1)^T e^{i\bar{\tau}\omega_0\theta},$$

where q_1 is a constant. Based on $A(0, 0)q(\theta) = i\bar{\tau}\omega_0 q(\theta)$, we have

$$\bar{\tau} \begin{pmatrix} -i\omega_0 & 1 \\ \frac{\alpha\beta}{m} & \bar{\eta}_1 e^{-i\omega_0} - i\omega_0 \end{pmatrix} q(0) = \begin{pmatrix} 0 \\ 0 \end{pmatrix}.$$

Thus, we can easily obtain $q_1 = i\omega_0$. Similarly, $q_1^* = -\frac{\alpha\beta}{m(i\omega_0 + \bar{\eta}_1 e^{-i\omega_0})}$. For \bar{D} , from the inner product defined in (19), we have

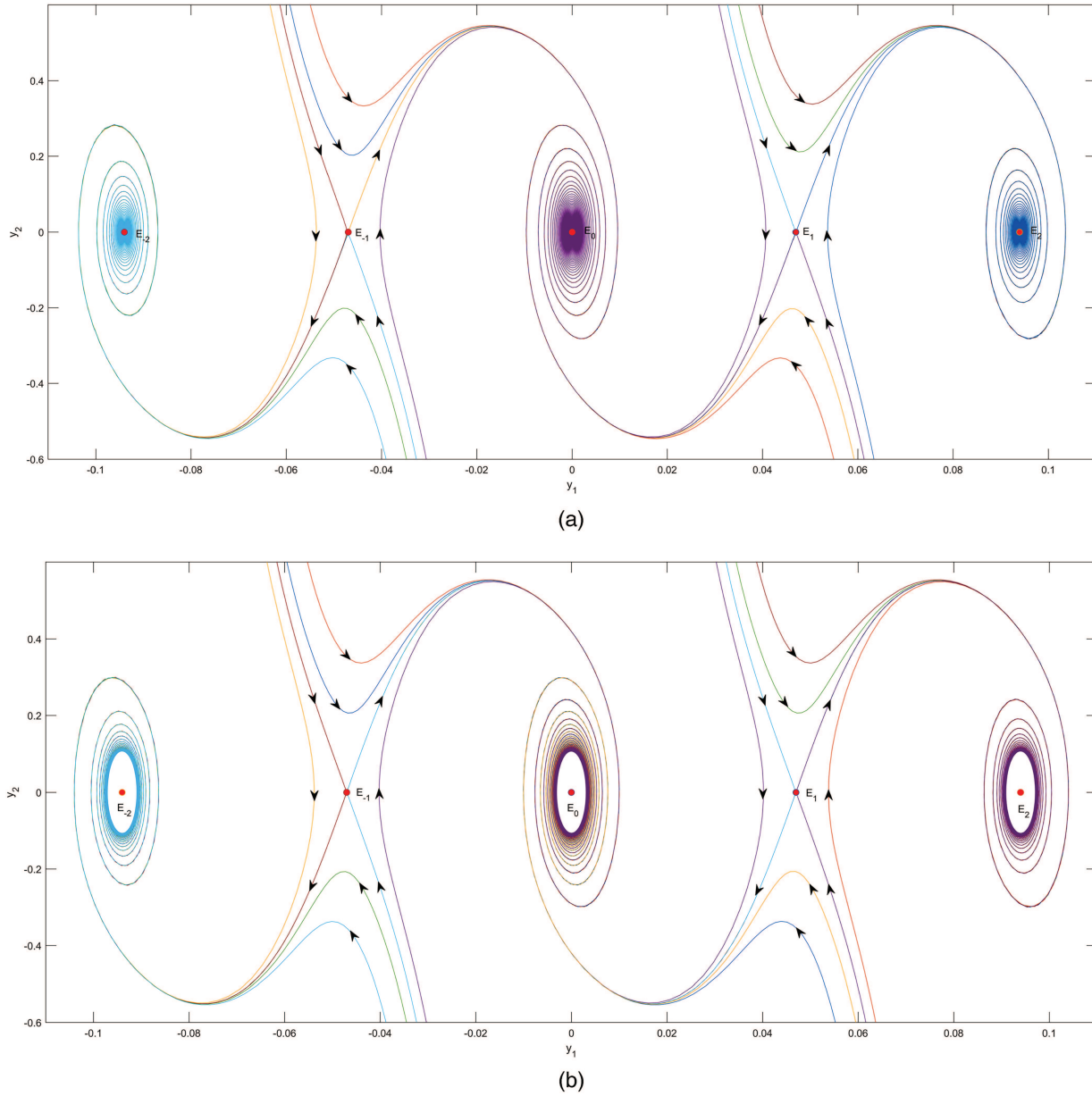


FIG. 2. Phase diagram of system (1) in $y_1 - y_2$ plane with different η_1 when $\alpha = -63$. (a) Three asymptotically stable solutions E_0 , E_1 , and E_{-2} , and two unstable saddle points E_1 and E_{-1} . (b) Three stable periodic solutions near E_0 , E_1 , and E_{-2} , and two unstable saddle points E_1 and E_{-1} . (a) $\eta_1 = -2$. (b) $\eta_1 = 3$.

$$\begin{aligned} \langle q^*(s), q(\theta) \rangle &= \bar{D}(1, \bar{q}_1^*)(1, q_1)^T - \int_{-1}^0 \int_0^\theta \bar{D}(1, \bar{q}_1^*) e^{-i\bar{\tau}\omega_0(\xi-\theta)} d\eta \\ &\quad \times (\theta, 0, 0)(1, q_1)^T e^{i\bar{\tau}\omega_0\xi} d\xi \\ &= \bar{D}(1 + q_1 \bar{q}_1^* - \int_{-1}^0 (1, \bar{q}_1^*) \theta e^{i\bar{\tau}\omega_0\theta} d\eta)(\theta, 0, 0)(1, q_1)^T \\ &= \bar{D}(1 + q_1 \bar{q}_1^* - \bar{\tau} \bar{\eta}_1 q_1 e^{-i\bar{\tau}\omega_0}). \end{aligned}$$

Thus, $\langle \psi, A\phi \rangle = \langle A^*\psi, \phi \rangle$ holds when

$$\bar{D} = \frac{1}{1 + q_1 \bar{q}_1^* - \bar{\tau} \bar{\eta}_1 q_1 e^{-i\bar{\tau}\omega_0}}.$$

At the same time, it is easy to verify that $\langle q^*(s), \bar{q}(\theta) \rangle = 0$. \square

Now, we need to introduce some symbols to compute the coordinates for the center manifold C_0 at $(\mu, \varsigma) = (0, 0)$. Note that

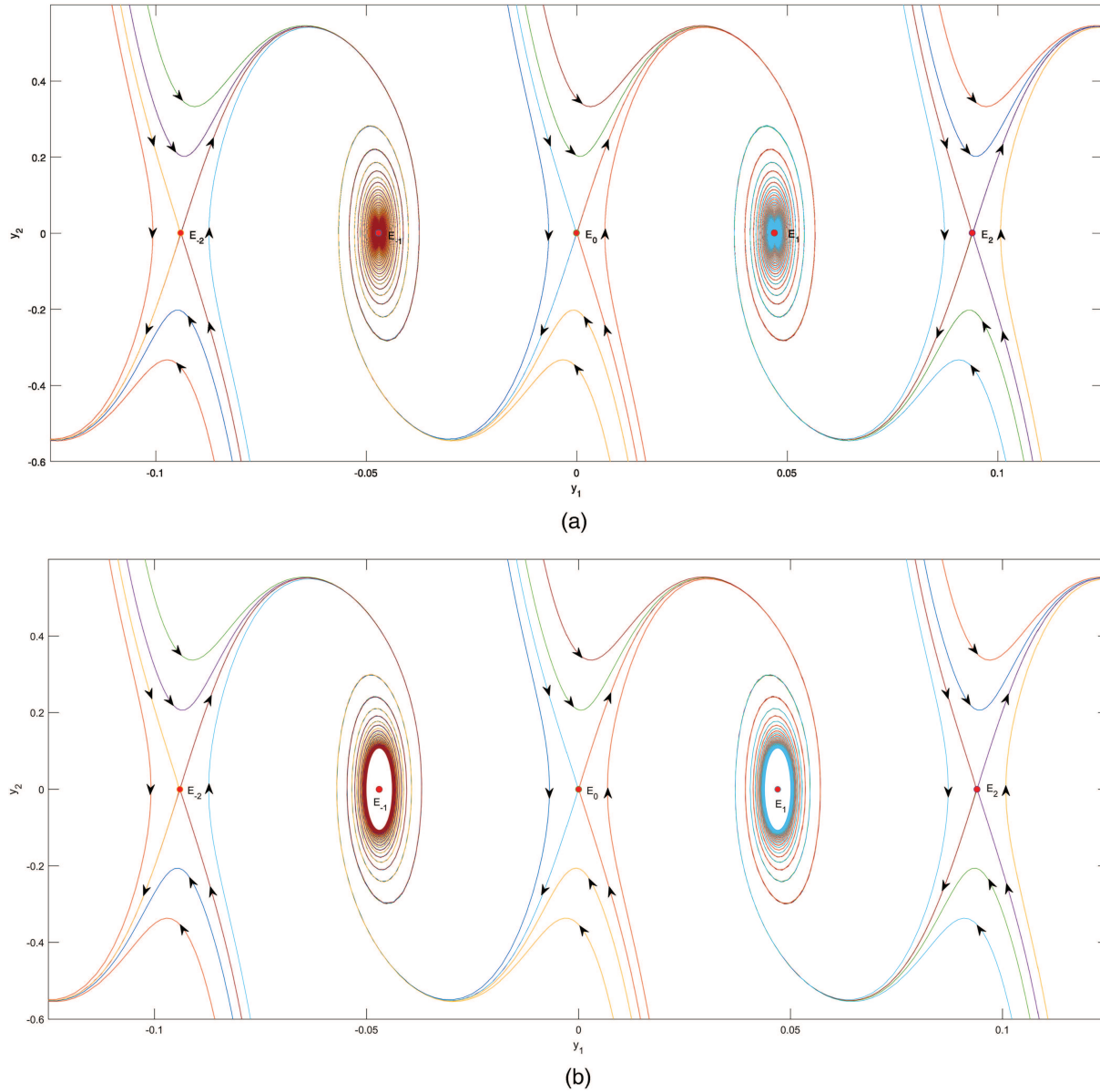


FIG. 3. Phase diagram of system (1) in $y_1 - y_2$ plane with different η_1 when $\alpha = 63$. (a) Two asymptotically stable solutions E_1 and E_{-1} , and three unstable saddle points E_0 , E_2 , and E_{-2} . (b) Two stable periodic solutions near E_1 and E_{-1} , respectively, and three unstable saddle points E_0 , E_2 and E_{-2} . (a) $\eta_1 = -2$. (b) $\eta_1 = 3$.

$z(t) = \langle q^*, u_t \rangle$ and

$$W(z, \bar{z}, \theta) = u_t(\theta) - 2 \operatorname{Re}[z(t)q(\theta)], \quad (20)$$

on the center manifold C_0 , actually,

$$\begin{aligned} W(z(t), \bar{z}(t), \theta) &= W_{20} \frac{z^2}{2} + W_{11} z \bar{z} + W_{02} \frac{\bar{z}^2}{2} + W_{12} z \bar{z}^2 \\ &\quad + W_{21} z^2 \bar{z} + W_{30} \frac{\bar{z}^3}{6} + h.o.t. \end{aligned}$$

Obviously, considering only the real solutions, we have

$$\begin{aligned} \dot{z}(t) &= \langle q^*, u_t \rangle = \langle q^*, A u_t + R u_t \rangle \\ &= \langle A^* q^*, u_t \rangle + \langle q^*, R u_t \rangle \\ &= i\omega_0 z + \bar{q}^*(0) F(0, W(t, \theta) + 2 \operatorname{Re}[z(t)q(0)]) \\ &= i\omega_0 z + g(z, \bar{z}), \end{aligned} \quad (21)$$

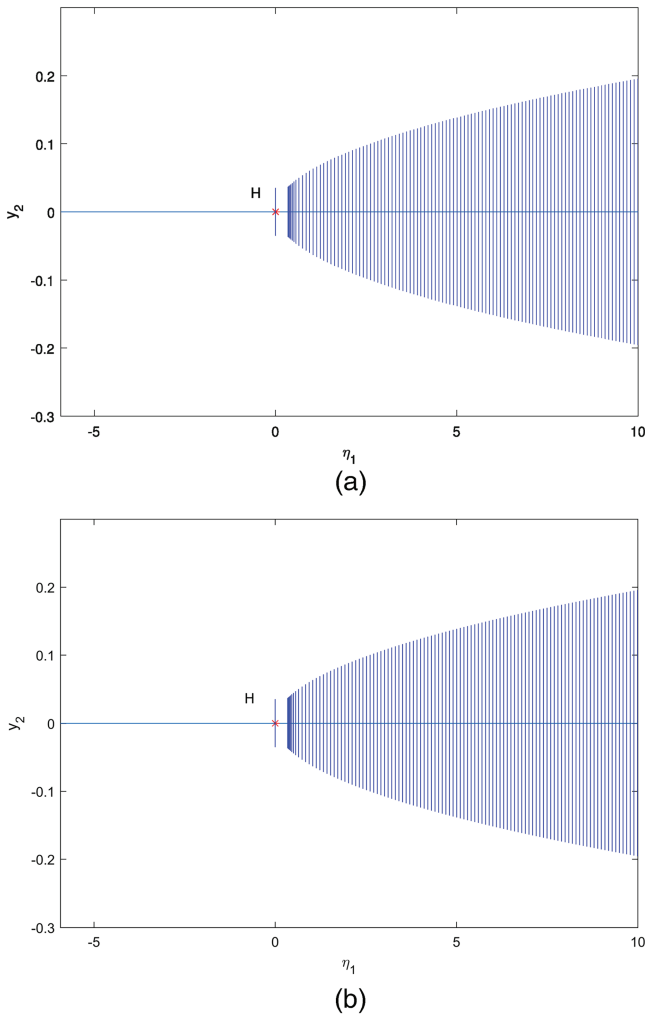


FIG. 4. Bifurcation diagram in $\eta_1 - y_2$ plane with different α . Both are stable limit cycle bifurcated from Hopf bifurcation. (a) $\alpha = -63$. (b) $\alpha = 63$.

where

$$g(z, \bar{z}) = g_{20} \frac{z^2}{2} + g_{11} z\bar{z} + g_{02} \frac{\bar{z}^2}{2} + g_{21} \frac{z^2\bar{z}}{2} + h.o.t. \quad (22)$$

Transforming Eq. (20) gives

$$\begin{aligned} u_t(\theta) &= W(z, \bar{z}, \theta) + 2 \operatorname{Re} \{z(t)q(\theta)\} \\ &= W(z, \bar{z}, \theta) + z(t)q(\theta) + \bar{z}(t)\bar{q}(\theta), \end{aligned}$$

and due to the form of $F(\mu, \varsigma, \phi)$, only setting $\theta = 0$, and defining $u_t = (u_{1t}(\theta), u_{2t}(\theta))^T$, we have

$$\begin{cases} u_{1t}(0) = z + \bar{z} + W_{20}^{(1)}(0) \frac{z^2}{2} \\ \quad + W_{11}^{(1)}(0)z\bar{z} + W_{02}^{(1)}(0) \frac{\bar{z}^2}{2} + \dots, \\ u_{2t}(0) = q_1 z + \bar{q}_1 \bar{z} + W_{20}^{(2)}(0) \frac{z^2}{2} \\ \quad + W_{11}^{(2)}(0)z\bar{z} + W_{02}^{(2)}(0) \frac{\bar{z}^2}{2} + \dots. \end{cases} \quad (23)$$

From (21), the expression of $g(z, \bar{z})$ is

$$\begin{aligned} g(z, \bar{z}) &= \bar{q}_1^*(0)F(0, W(z, \bar{z}, \theta) + 2 \operatorname{Re}[z(t)q(0)]) \\ &= \bar{D}\bar{\tau}(1, \bar{q}_1^*) \left(\begin{array}{c} 0 \\ -\frac{1}{6}\beta^3 u_{1t}^3(0) + \frac{\eta_2}{m} u_{2t}^3(0) \end{array} \right) \\ &= \bar{D}\bar{\tau} \left(-\frac{1}{6}\bar{q}_1^*\beta^3 u_{1t}^3(0) + \frac{\eta_2}{m} \bar{q}_1^* u_{2t}^3(0) \right). \end{aligned} \quad (24)$$

Substituting (23) into (24) and comparing the coefficients with (22) yields

$$\begin{aligned} g_{20} &= g_{11} = g_{02} = 0, \\ g_{21} &= -\bar{q}_1^*\beta^3 + 6\frac{\eta_2}{m}\bar{q}_1^*q_1^2\bar{q}_1, \\ g_{12} &= -\bar{q}_1^*\beta^3 + 6\frac{\eta_2}{m}\bar{q}_1^*q_1\bar{q}_1^2, \\ g_{03} &= -\bar{q}_1^*\beta^3 + 6\frac{\eta_2}{m}\bar{q}_1^*\bar{q}_1^3, \\ g_{30} &= -\bar{q}_1^*\beta^3 + 6\frac{\eta_2}{m}\bar{q}_1^*q_1^3, \\ g_{40} &= -6\bar{q}_1^*\beta^3 W_{20}^{(1)}(0) + 36\frac{\eta_2}{m}\bar{q}_1^*q_1^2 W_{20}^{(2)}(0), \\ g_{13} &= -3\bar{q}_1^*\beta^3 \left(W_{11}^{(1)}(0) + \frac{W_{02}^{(1)}(0)}{2} \right) \\ &\quad + 18\bar{q}_1^*\frac{\eta_2}{m} \left(\bar{q}_1^2 W_{11}^{(2)}(0) + q_1 \bar{q}_1 \frac{W_{02}^{(2)}(0)}{2} \right), \\ g_{31} &= -3\bar{q}_1^*\beta^3 \left(W_{11}^{(1)}(0) + \frac{W_{20}^{(1)}(0)}{2} \right) \\ &\quad + 18\bar{q}_1^*\frac{\eta_2}{m} \left(q_1^2 W_{11}^{(2)}(0) + q_1 \bar{q}_1 \frac{W_{20}^{(2)}(0)}{2} \right), \\ g_{32} &= -6\bar{q}_1^*\beta^3 \left(\frac{W_{12}^{(1)}(0)}{2} + \frac{W_{21}^{(1)}(0)}{2} \right. \\ &\quad \left. + \frac{W_{20}^{(1)}(0)W_{02}^{(1)}(0)}{4} \right. \\ &\quad \left. + \left(W_{11}^{(1)}(0) \right)^2 + \frac{W_{20}^{(1)}(0)W_{11}^{(1)}(0)}{2} + \frac{W_{30}^{(1)}(0)}{6} \right) \\ &\quad + 36\bar{q}_1^*\frac{\eta_2}{m} \left(\frac{q_1^2 W_{12}^{(2)}(0)}{2} + \frac{q_1 \bar{q}_1 W_{21}^{(2)}(0)}{2} + \frac{q_1 W_{20}^{(2)}(0)W_{02}^{(2)}(0)}{4} \right. \\ &\quad \left. + q_1 \left(W_{11}^{(2)}(0) \right)^2 + \bar{q}_1 \frac{W_{20}^{(2)}(0)W_{11}^{(2)}(0)}{2} + \frac{\bar{q}_1^2 W_{30}^{(2)}(0)}{6} \right), \end{aligned}$$

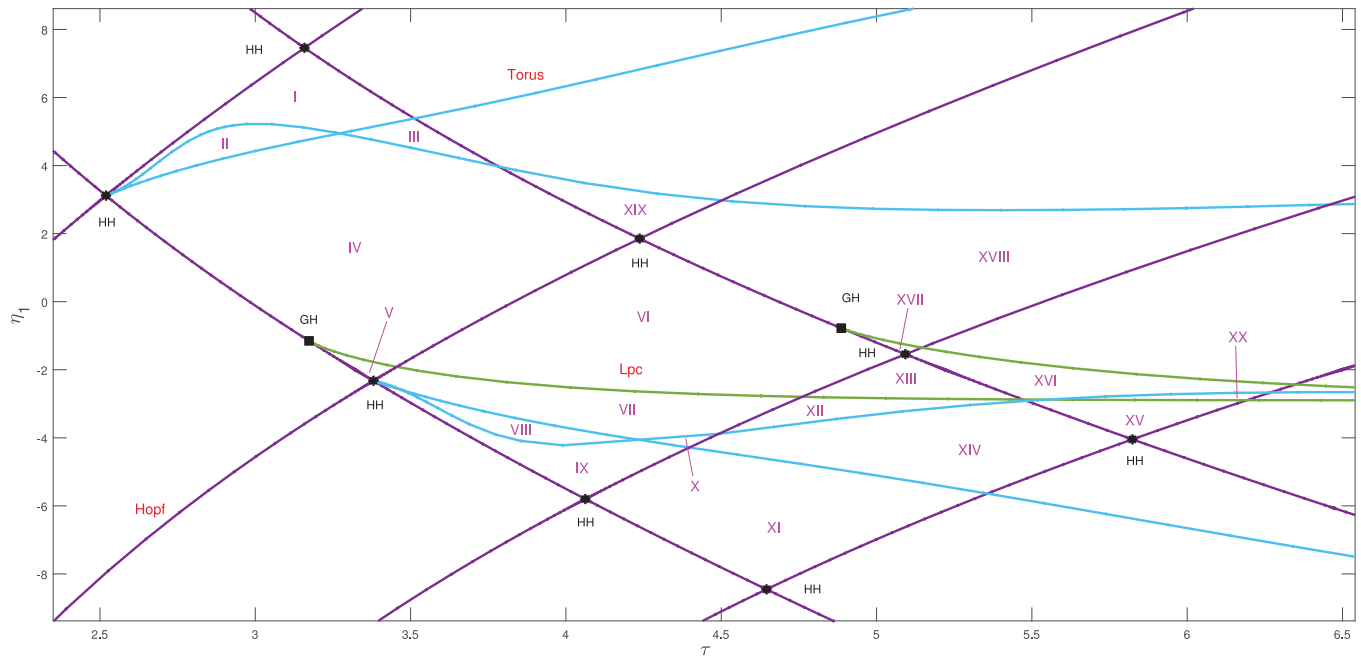


FIG. 5. Bifurcation diagram of system (2) in $\tau - \eta_1$ plane. The meaning of the curves are as follows: Hopf (purple); LPC (green) limit point of cycles; torus (cyan); special points are HH (Hopf-Hopf) and GH (Bautin).

$$\begin{aligned} g_{22} = & -2\bar{q}_1^* \beta^3 \left(W_{11}^{(1)}(0) + \frac{W_{02}^{(1)}(0)}{2} + \frac{W_{20}^{(1)}(0)}{2} \right) \\ & + 12\bar{q}_1^* \frac{\eta_2}{m} \left(q_1 \bar{q}_1 W_{11}^{(2)}(0) + \bar{q}_1^2 \frac{W_{20}^{(2)}(0)}{2} + q_1^2 \frac{W_{02}^{(2)}(0)}{2} \right). \end{aligned}$$

Remark 2. For the unknown $W_{11}^{(j)}(0)$, $W_{02}^{(j)}(0)$, $W_{20}^{(j)}(0)$, $W_{12}^{(j)}(0)$, $W_{30}^{(j)}(0)$, $j = 1, 2$ above, we know some initial conditions of the following differential equations:

$$\frac{dW}{dt} = \begin{cases} AW - q^*(0)F(0, u_t(\theta))q(\theta) & \text{for } -1 \leq \theta < 0, \\ AW - q^*(0)F(0, u_t(\theta))q(\theta) \\ + F(0, u_t(\theta)) & \text{for } \theta = 0. \end{cases}$$

By solving the above equation, we can get the final expression result, and the calculation process can refer to Refs. 27 and 28.

On the basis of previous analysis, the calculation results show that

$$\mu_2 = -\frac{\operatorname{Re}[C_1(0)]}{\operatorname{Re}[\lambda'(\tau_0)]}, \quad \beta_2 = 2\operatorname{Re}C_1(0),$$

where

$$C_1(0) = \frac{i}{2\omega_0} \left(g_{20}g_{11} - 2|g_{11}|^2 - \frac{1}{3}|g_{02}|^2 \right) + \frac{g_{21}}{2}.$$

Actually, the sign of μ_2 resolves the direction of the Hopf bifurcation and β_2 the stability of periodic solutions, so we have the below theorem.

Theorem 6. If $\mu_2 > 0$ ($\mu_2 < 0$), then the Hopf bifurcation is supercritical (subcritical) and the bifurcating periodic solutions on the center manifold are stable (unstable) if $\beta_2 < 0$ ($\beta_2 > 0$).

In fact, to illustrate the existence of the Bautin bifurcation, we need to calculate the first Lyapunov coefficient and the second Lyapunov coefficient as follows:

$$l_1(\mu, \varsigma) = \frac{1}{2\omega_0} \left[\operatorname{Re} g_{21} - \frac{1}{\omega_0} \operatorname{Im}(g_{20}g_{11}) \right]$$

and

$$\begin{aligned} 12l_2(0, 0) = & \frac{1}{\omega_0} \operatorname{Re} g_{32} + \frac{1}{\omega_0^2} \operatorname{Im} [g_{20}\bar{g}_{31} - g_{11}(4g_{31} + 3\bar{g}_{22}) \\ & - \frac{1}{3}g_{02}(g_{40} + \bar{g}_{13}) - g_{30}g_{12}] \\ & + \frac{1}{\omega_0^3} \operatorname{Re} \left[g_{20}\bar{g}_{11}(3g_{12} - \bar{g}_{30}) + g_{20}g_{02} \left(\bar{g}_{12} - \frac{1}{3}g_{30} \right) \right. \\ & \left. + \frac{1}{3}g_{20}\bar{g}_{02}g_{30} + g_{11}\bar{g}_{02} \left(\frac{5}{3}\bar{g}_{30} + 3g_{12} \right) \right] \\ & + \frac{1}{\omega_0^3} \operatorname{Re} \left[\frac{1}{3}g_{11}g_{02}\bar{g}_{03} - 4g_2^{11}g_{30} \right] \\ & + \frac{3}{\omega_0^3} \operatorname{Im}(g_{20}g_{11}) \operatorname{Im} g_{21} \end{aligned}$$

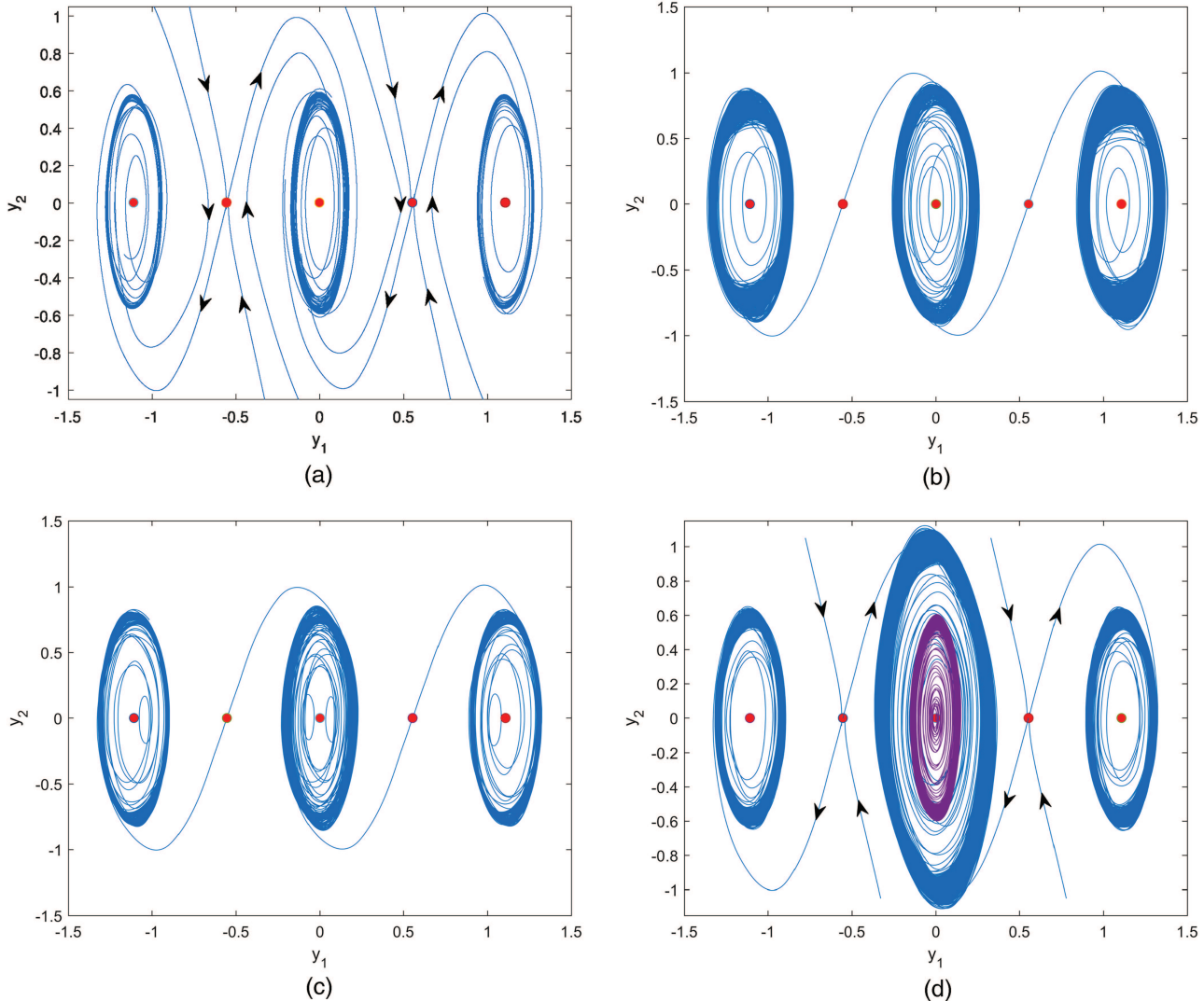


FIG. 6. Numerical results for system (2) in regions IV, XIX, XIV, and VII of Fig. 5. (a)–(c) Three stable periodic solutions near E_0 and E_2 and E_{-2} , and two unstable saddle points E_1 and E_{-1} . (d) Four stable periodic solutions, two of which coexist near equilibrium point E_0 , and two unstable saddle points. (a) IV: $(\tau, \eta_1) = (3.7, 1.8)$. (b) VII: $(\tau, \eta_1) = (4.2, -3)$. (c) VII: $(\tau, \eta_1) = (3.8, -3.4)$. (d) XIX: $(\tau, \eta_1) = (4.2, 3)$.

$$\begin{aligned} &+ \frac{1}{\omega_0^4} \operatorname{Im} [g_{11}\bar{g}_{02}(\bar{g}_{20}^2 - 3\bar{g}_{20}g_{11} - 4g_{11}^2)] \\ &+ \frac{1}{\omega_0^4} \operatorname{Im}(g_{20}g_{11}) [3\operatorname{Re}(g_{20}g_{11}) - 2|g_{02}|^2]. \end{aligned}$$

For transversality condition, obviously, if $\frac{\partial l_1(\mu, \varsigma)}{\partial \varsigma} \neq 0$, then the map $(\mu, \varsigma) \rightarrow (\frac{\xi(\mu)}{\omega(\mu)}, l_1(\mu, \varsigma))$ near $(\mu, \varsigma) = (0, 0)$ is

$$\begin{pmatrix} \frac{\partial \frac{\xi(\mu)}{\omega(\mu)}}{\partial \mu} & \frac{\partial \frac{\xi(\mu)}{\omega(\mu)}}{\partial \varsigma} \\ \frac{\partial l_1(\mu, \varsigma)}{\partial \mu} & \frac{\partial l_1(\mu, \varsigma)}{\partial \varsigma} \end{pmatrix} \neq 0.$$

Theorem 7. System (2) undergoes a Bautin bifurcation at critical point $(\bar{\tau}, \bar{\eta}_1)$, when $l_1(0, 0) = 0$, $\frac{\partial l_1(\mu, \varsigma)}{\partial \varsigma} \neq 0$ and $l_2(0, 0) \neq 0$ hold.

V. HOPF-HOPF BIFURCATION IN SYSTEM (2)

In this section, Hopf-Hopf bifurcation is considered in delayed high-temperature superconducting maglev model (2). Hopf-Hopf bifurcation requires that characteristic equation (11) has two pairs of purely imaginary roots. In fact, Lemma 1 has given the conditions for two pairs of purely imaginary roots, which we write

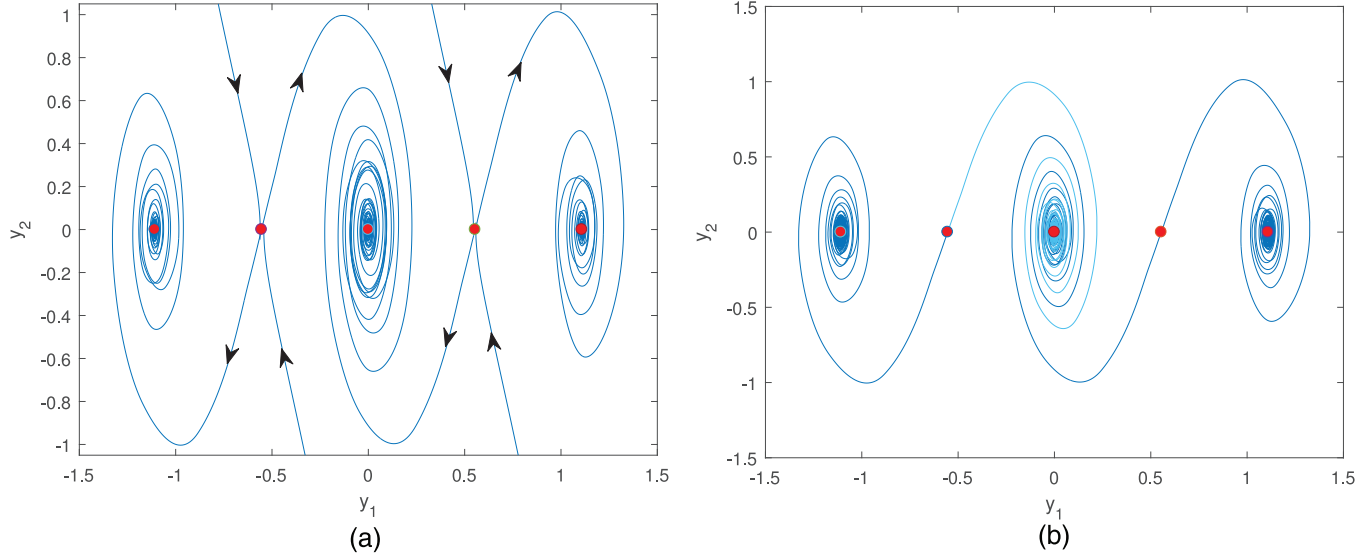


FIG. 7. Numerical results for system (2) in regions IV, V, XIX, XIV, and VII, XVII of Fig. 5. (a) and (b) Three asymptotically stable solutions \$E_0\$, \$E_2\$ and \$E_{-2}\$, and two unstable saddle points \$E_1\$ and \$E_{-1}\$. (a) IV: \$(\tau, \eta_1) = (3.7, 1.8)\$. (b) V: \$(\tau, \eta_1) = (3.34, -1.8)\$.

down as \$\pm i\omega_1\$ and \$\pm i\omega_2\$ here, and still use the perturbation symbol \$\mu = \tau - \bar{\tau}\$, \$\varsigma = \eta_1 - \bar{\eta}_1\$ in Sec. IV.

\$A(0, 0)\$ has two eigenvectors \$p_1, p_2\$ corresponding to the eigenvalues \$i\omega_1, -i\omega_2\$, respectively, and the adjoint eigenvectors for \$A^*\$ are \$p_1^*, p_2^*\$, respectively. From Lemma 2, we can know that these eigenvectors have the following forms:

$$\begin{aligned} p_1(\theta) &= (1, \gamma_1)^T e^{i\omega_1 \theta}, & p_1^*(s) &= D_1(1, \gamma_1^*)^T e^{i\omega_1 s}, \\ p_2(\theta) &= (1, \gamma_2)^T e^{i\omega_2 \theta}, & p_2^*(s) &= D_2(1, \gamma_2^*)^T e^{i\omega_2 s}, \end{aligned}$$

with

$$\begin{cases} \langle p_j^*, p_k \rangle = 1 & \text{if } j = k, \\ \langle p_j^*, p_k \rangle = 0 & \text{if } j \neq k, \end{cases}$$

where

$$\gamma_j = i\omega_j, \quad \gamma_j^* = -\frac{\alpha\beta}{m(i\omega_j + \bar{\eta}_1 e^{-i\omega_j})},$$

$$\bar{D}_j = \frac{1}{1 + \gamma_j \bar{\gamma}_j^* - \bar{\tau} \bar{\eta}_1 \gamma_j e^{-i\bar{\tau}\omega_j}}, \quad j = 1, 2.$$

Define \$Z_j(t) = \langle p_j^*, u_t \rangle\$ and

$$W(t, \theta) = u_t(\theta) - 2 \operatorname{Re}[Z_1(t)p_1(\theta) + Z_2(t)p_2(\theta)]. \quad (25)$$

On the center manifold \$C_0\$, one has

$$\begin{aligned} \dot{Z}_1(t) &= \langle p_1^*, \dot{u}_t \rangle \\ &= \langle p_1^*, A u_t + R u_t \rangle \\ &= i\omega_1 Z_1(t) + \bar{p}_1^*(0) F(0, W(t, \theta)) \\ &\quad + 2 \operatorname{Re}[Z_1(t)p_1(0) + Z_2(t)p_2(0)] \\ &= i\omega_1 Z_1(t) + h^1(Z_1(t), \bar{Z}_1(t), Z_2(t), \bar{Z}_2(t)), \\ \dot{Z}_2(t) &= \langle p_2^*, \dot{u}_t \rangle \\ &= \langle p_2^*, A u_t + R u_t \rangle \\ &= i\omega_2 Z_1(t) + \bar{p}_2^*(0) F(0, W(t, \theta)) \\ &\quad + 2 \operatorname{Re}[Z_1(t)p_1(0) + Z_2(t)p_2(0)] \\ &= i\omega_2 Z_1(t) + h^2(Z_1(t), \bar{Z}_1(t), Z_2(t), \bar{Z}_2(t)), \end{aligned}$$

where

$$\begin{aligned} h^j(Z_1(t), Z_2(t), \bar{Z}_1(t), \bar{Z}_2(t)) \\ = \sum_{l+s+r+k \geq 1} \frac{1}{l!s!r!k!} h_{lsrk}^j Z_1^l \bar{Z}_1^s Z_2^r \bar{Z}_2^k, \quad j = 1, 2. \end{aligned} \quad (26)$$

From (25), we have

$$\begin{aligned} u_t(\theta) &= W(t, \theta) + 2 \operatorname{Re}[Z_1(t)p_1(\theta) + Z_2(t)p_2(\theta)] \\ &= W(t, \theta) + Z_1(t)p_1(\theta) + \bar{Z}_1(t)\bar{p}_1(\theta) + Z_2(t)p_2(\theta) \\ &\quad + \bar{Z}_2(t)\bar{p}_2(\theta). \end{aligned}$$

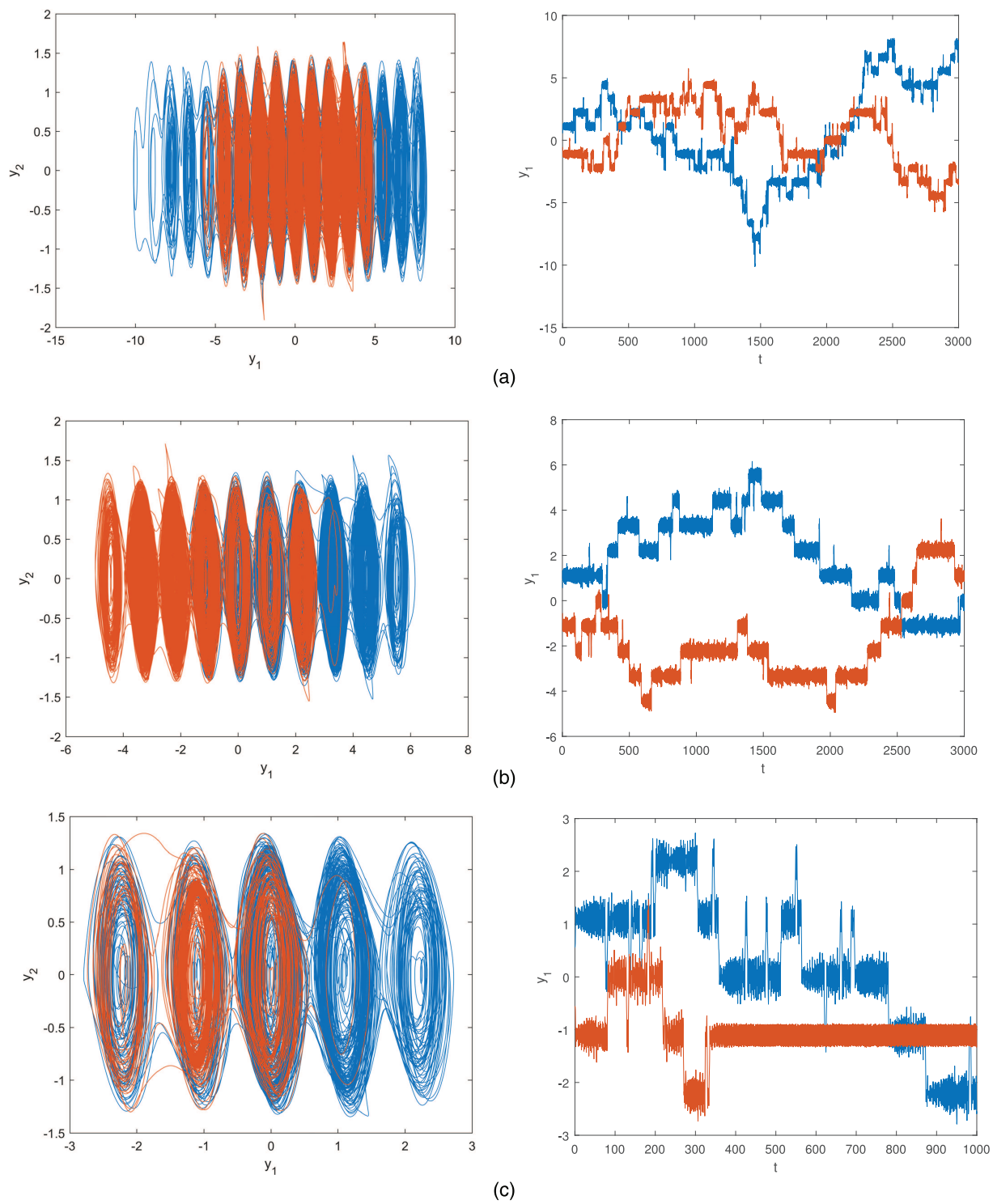


FIG. 8. Numerical results for system (2) in regions IX, X, and X/IV of Fig. 5. (a) IX: $(\tau, \eta_1) = (4.05, -4.5)$. (b) X: $(\tau, \eta_1) = (4.4, -4.1)$. (c) X/IV: $(\tau, \eta_1) = (5.2, -4)$.

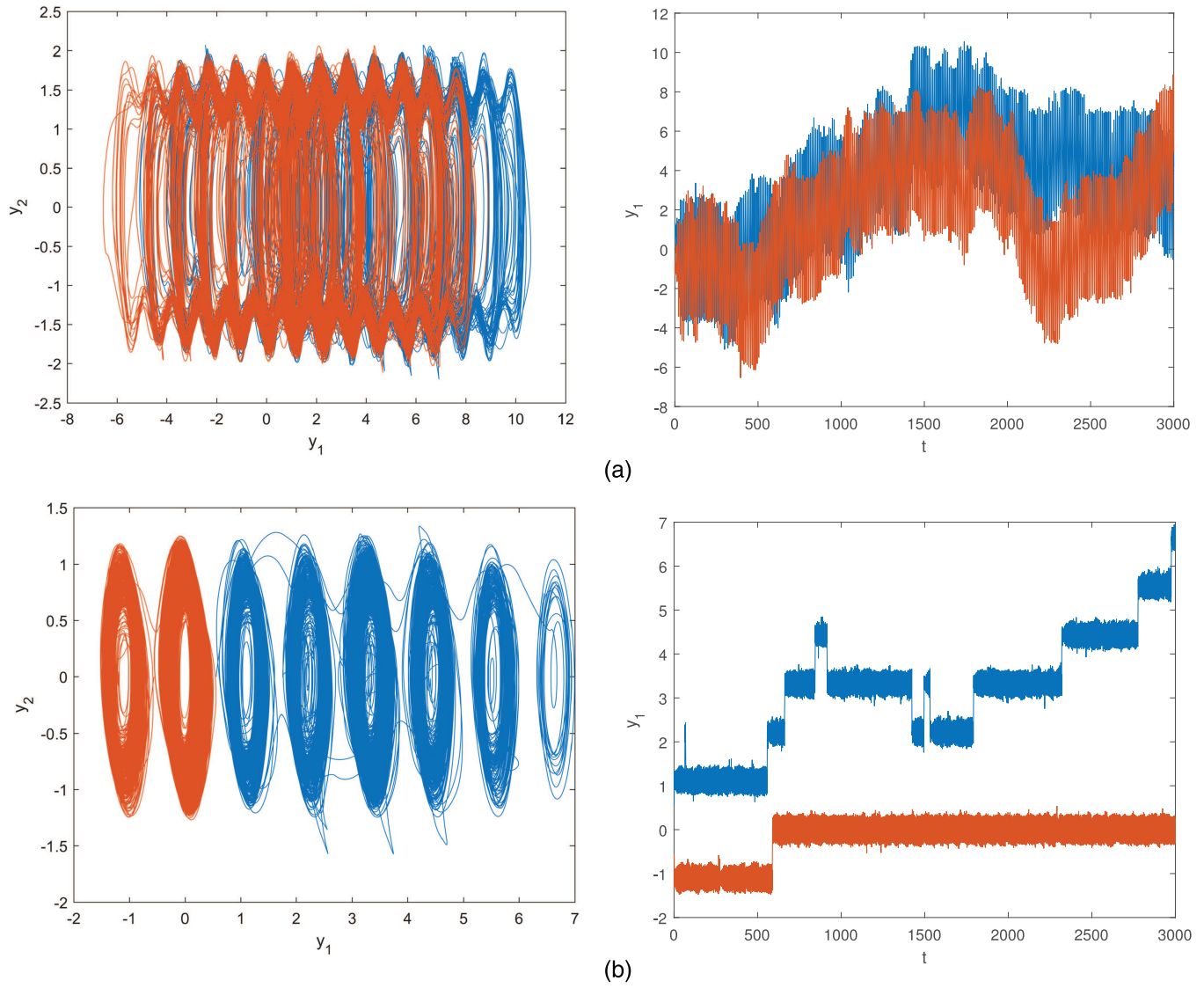


FIG. 9. Numerical results for system (2) in regions XI, XII, and XIV of Fig. 5. (a) XI: $(\tau, \eta_1) = (4.7, -7)$. (b) XII: $(\tau, \eta_1) = (4.75, -3.4)$.

Further,

$$\begin{cases} u_{1t}(0) = Z_1 + Z_2 + \bar{Z}_1 + \bar{Z}_2 \\ \quad + \sum_{l+s+r+k \geq 2} W_{lsrk}^{(1)}(0) \frac{Z_1^l Z_2^r \bar{Z}_1^s \bar{Z}_2^k}{l! s! r! k!}, \\ u_{2t}(0) = \gamma_1 Z_1 + \gamma_2 Z_2 + \bar{\gamma}_1 \bar{Z}_1 + \bar{\gamma}_2 \bar{Z}_2 \\ \quad + \sum_{l+s+r+k \geq 2} W_{lsrk}^{(2)}(0) \frac{Z_1^l Z_2^r \bar{Z}_1^s \bar{Z}_2^k}{l! s! r! k!}. \end{cases}$$

On the other hand, $h^j(Z_1, Z_2, \bar{Z}_1, \bar{Z}_2)$ has a form similar to (24),

$$\begin{aligned} h^j(Z_1, Z_2, \bar{Z}_1, \bar{Z}_2) &= \bar{D}_j \bar{\tau}(1, \gamma_j^*) \begin{pmatrix} 0 \\ -\frac{1}{6} \beta^3 u_{1t}^3(0) + \frac{\eta_2}{m} u_{2t}^2(0) \end{pmatrix} \\ &= \begin{pmatrix} -\frac{1}{6} \bar{D}_1 \bar{\tau} \beta^3 \gamma_1^* u_{1t}^3(0) + \frac{\eta_2}{m} \bar{D}_1 \bar{\tau} \gamma_1^* u_{2t}^3(0) \\ -\frac{1}{6} \bar{D}_2 \bar{\tau} \beta^3 \gamma_2^* u_{1t}^3(0) + \frac{\eta_2}{m} \bar{D}_2 \bar{\tau} \gamma_2^* u_{2t}^3(0) \end{pmatrix}. \end{aligned} \quad (27)$$

Comparing the coefficients of (26) and (27), the key coefficient of normal form can be obtained,

$$h_{1002}^1 = -\bar{D}_1 \bar{\tau} \beta^3 \gamma_1^* + \frac{\eta_2}{m} \bar{D}_1 \bar{\tau} \gamma_1^* \gamma_1 \bar{\gamma}_2^2,$$

$$\begin{aligned} h_{2100}^1 &= -\bar{D}_1 \bar{\tau} \beta^3 \gamma_1^* + 6 \frac{\eta_2}{m} \bar{D}_1 \bar{\tau} \gamma_1^* \gamma_1^2 \bar{\gamma}_1, \\ h_{1011}^1 &= -\frac{1}{2} \bar{D}_1 \bar{\tau} \beta^3 \gamma_1^* + 3 \frac{\eta_2}{m} \bar{D}_1 \bar{\tau} \gamma_1^* \gamma_1 \gamma_2 \bar{\gamma}_2, \\ h_{1110}^2 &= -\bar{D}_2 \bar{\tau} \beta^3 \gamma_2^* + 6 \frac{\eta_2}{m} \bar{D}_2 \bar{\tau} \gamma_2^* \gamma_1 \bar{\gamma}_1 \gamma_2, \\ h_{2100}^2 &= -\bar{D}_2 \bar{\tau} \beta^3 \gamma_2^* + 6 \frac{\eta_2}{m} \bar{D}_2 \bar{\tau} \gamma_2^* \gamma_1^2 \bar{\gamma}_1, \\ h_{0021}^2 &= -\frac{1}{2} \bar{D}_2 \bar{\tau} \beta^3 \gamma_2^* + 3 \frac{\eta_2}{m} \bar{D}_2 \bar{\tau} \gamma_2^* \gamma_2^2 \bar{\gamma}_2. \end{aligned}$$

So, the third-order normal form near a Hopf–Hopf point $(\bar{\tau}, \bar{\eta}_1)$ is decided by

$$\begin{cases} \dot{Z}_1 = i\omega_1 Z_1 + h_{2100}^1 Z_1^2 \bar{Z}_1 + h_{1011}^1 Z_1 Z_2 \bar{Z}_2 + h_{1002}^1 Z_1 \bar{Z}_2^2 + h.o.t, \\ \dot{Z}_2 = i\omega_2 Z_2 + h_{1110}^2 Z_1 \bar{Z}_1 Z_2 + h_{0021}^2 Z_2^2 \bar{Z}_2 + h_{2100}^2 Z_1^2 \bar{Z}_1 + h.o.t. \end{cases}$$

Remark 3. After further scaling, a more concise amplitude equation can be obtained

$$\begin{cases} \dot{r}_1 = r_1(a_1 + r_1^2 + b_1 r_2^2), \\ \dot{r}_2 = r_2(c_1 + d_1 r_1^2 + e_1 r_2^2). \end{cases}$$

The types of Hopf–Hopf bifurcation are distinguished by the coefficient symbol of normal form (see Ref. 26 for details).

VI. NUMERICAL SIMULATIONS

The Hopf bifurcation is accompanied by stable or unstable periodic solutions, while the Hopf–Hopf bifurcation leads to the coexistence of multiple periods. In this section, we simulate the Hopf bifurcation of system (1) and the co-dimension two bifurcations of system (2).

Looking into Eq. (6), it is easy to know that $\eta_1=0$ is a critical value for the system to undergo a Hopf bifurcation at zero equilibrium point E_0 . In fact, the stability of the system is simulated in Ref. 20 but the Hopf bifurcation and its periodic solution as well as the stability transformation of odd and even equilibrium points are not involved. For example, we take η_1 as the bifurcation parameter and select the following parameter values:

$$\alpha = -63, \beta = 66.84, \eta_2 = -350, m = 3.5.$$

Some calculations show $\frac{\alpha\beta}{m} = -1203.12 < 0$. From Theorem 4, we know that system (1) undergoes a Hopf bifurcation at zero equilibrium point E_0 , as shown in Fig. 2. It can be seen from Fig. 2 that when $\eta_1 = -2$, the zero equilibrium point of the system is asymptotically stable. In fact, in this case, all even equilibrium points are asymptotically stable, while odd equilibrium points are unstable saddle points, which means that if the vehicle is not disturbed, it can only theoretically maintain the nearest equilibrium position. When there is a disturbance, the vehicle may enter different stable or unstable regions or even enter another from one region. If the vehicle always runs in a stable region, it will eventually return to the equilibrium position, and if the vehicle moves into an unstable region, it will eventually derail or even overturn. However, the phenomenon in Fig. 3 is completely opposite to that in Fig. 2. The Hopf bifurcation

occurs at the odd equilibrium point of the system, and the even equilibrium point becomes an unstable saddle point. The corresponding Hopf bifurcation diagram of Figs. 2 and 3 is shown in Fig. 4.

For the delay model (2), to comprehensively illustrate the abundant co-dimension two bifurcation of the system, we first give the two-parameter (τ and η_1) bifurcation diagram of the system by using DDE-biftool software package^{29–31} and divide it into different regions (see Fig. 5). In Fig. 5, the parameter values we selected are as follows:

$$\alpha = -6, \beta = 5.6684, \eta_2 = -3, m = 2.5.$$

From the figure, we can know that the intersection of Hopf bifurcation curves makes Hopf–Hopf bifurcations occur in the system, and the region is, therefore, presented as a regular grid. There are two Torus bifurcation curves originating from Hopf–Hopf points at the top corner of each grid. There are Bautin bifurcations on the two Hopf bifurcations from top left to bottom right, accompanied by two limit point of cycles originating from Bautin points, respectively. When the time delay is small, the asymptotically stable solution or periodic solution (similar to Fig. 2) appears at the nearest equilibrium point of the system, as shown in Figs. 6 and 7. The more interesting phenomenon is that when the parameter value is set in XIX, two periodic solutions coexist near the equilibrium point E_0 , which increases the stable state of the vehicle. However, with the increase in delay, the large-scale continuous stability region of the system is destroyed and turns into intermittent stability or instability (the solution eventually extends infinitely in the positive or negative direction) (see Figs. 8 and 9). At the same time, more complex chaotic behavior is generated, which shows that the vehicle will not operate normally and is more likely to derail.

VII. CONCLUSION

This paper studies a high-temperature superconducting maglev model with guidance force from the perspective of bifurcation and stability. For ordinary differential models, the Hopf bifurcation and its properties are investigated, and the stability transformation of odd and even equilibrium points is also studied. For the delayed model, we analyze the Hopf–Hopf bifurcation and Bautin bifurcation and simulate the key parameter region based on the two-parameter bifurcation diagram. Compared with the ordinary differential model, the dynamic properties of the delayed model are more complex, such as periodic coexistence, chaos, etc., which provides a new research direction for exploring the steady state of the high-temperature superconducting maglev model. For example, in the actual driving process, try to reduce the vehicle speed delay so as to better maintain the stability of the whole system.

ACKNOWLEDGMENTS

The author is grateful to all anonymous reviewers for their valuable comments, which has provided great help for the improvement of the paper.

AUTHOR DECLARATIONS

Conflict of Interest

The authors have no conflicts to disclose.

Author Contributions

Qinrui Dai: Methodology (equal); Software (equal); Writing – review & editing (equal).

DATA AVAILABILITY

The data that support the findings of this study are available within the article.

REFERENCES

- ¹J. Wang, S. Wang, and J. Zheng, “Recent development of high temperature superconducting maglev system in China,” *IEEE Trans. Appl. Supercond.* **19**, 2142–2147 (2009).
- ²H. Li, D. Liu, Y. Hong, J. Yu, J. Zheng, and Z. Deng, “Modeling and identification of the hysteresis nonlinear levitation force in HTS maglev systems,” *Supercond. Sci. Technol.* **33**, 054001 (2020).
- ³W. Hong, Y. Xin, C. Wang, Y. Wen, C. Zhao, and W. Li, “Technical feasibility study of an E-shaped electromagnetic guideway for HTS maglev,” *IEEE Trans. Appl. Supercond.* **30**, 1–10 (2020).
- ⁴Z. Deng, L. Wang, H. Li, J. Li, H. Wang, and J. Yu, “Dynamic studies of the HTS maglev transit system,” *IEEE Trans. Appl. Supercond.* **31**, 1–5 (2021).
- ⁵L. Jin, J. Zheng, H. Li, J. Li, Z. Zhou, Y. Zhang, and Z. Deng, “Effect of eddy current damper on the dynamic vibration characteristics of high-temperature superconducting maglev system,” *IEEE Trans. Appl. Supercond.* **27**, 1–6 (2017).
- ⁶S. Wang, J. Wang, C. Deng, Y. Lu, Y. Zeng, H. Song, H. Huang, H. Jing, Y. Huang, J. Zheng *et al.*, “An update high-temperature superconducting maglev measurement system,” *IEEE Trans. Appl. Supercond.* **17**, 2067–2070 (2007).
- ⁷Z. Deng, W. Zhang, J. Zheng, B. Wang, Y. Ren, X. Zheng, and J. Zhang, “A high-temperature superconducting maglev-evacuated tube transport (HTS maglev-ETT) test system,” *IEEE Trans. Appl. Supercond.* **27**, 1–8 (2017).
- ⁸X. Zhao, S. Tang, Y. Liu, and L. Yang, “Analysis to the forced vibration of a high temperature superconducting system with hysteresis,” *IEEE Trans. Appl. Supercond.* **30**, 1–5 (2020).
- ⁹Z. Yu, G. Zhang, Q. Qiu, D. Zhang, X. Sun, S. Wang, Y. Liu, W. Feng, W. Li, and L. Ai, “Electromagnetic and rotational characteristics of a superconducting flywheel energy storage system utilizing a radial-type high-temperature superconducting bearing,” *J. Supercond. Nov. Magn.* **32**, 1605–1616 (2019).
- ¹⁰Q. Li, Z. Deng, L. Wang, H. Li, J. Zhang, and E. F. Rodriguez, “Active vibration control of secondary suspension based on high-temperature superconducting maglev vehicle system,” *Physica C* **585**, 1353872 (2021).
- ¹¹L. Wang, Z. Deng, Y. Li, and H. Li, “Vertical-lateral coupling force relation of the high-temperature superconducting magnetic levitation system,” *IEEE Trans. Appl. Supercond.* **31**, 1–6 (2020).
- ¹²L. Chen, Z. Deng, B. Deng, and J. Zheng, “Numerical simulations on the vertical dynamic characteristics of high-temperature superconducting bulk,” *J. Supercond. Nov. Magn.* **34**, 683–694 (2021).
- ¹³J. Li, H. Li, J. Zheng, B. Zheng, H. Huang, and Z. Deng, “Nonlinear vibration behaviors of high-T_c superconducting bulks in an applied permanent magnetic array field,” *J. Appl. Phys.* **121**, 243901 (2017).
- ¹⁴C. Navau, A. Sanchez, and E. Pardo, “Lateral force in permanent magnet-superconductor levitation systems with high critical current,” *IEEE Trans. Appl. Supercond.* **13**, 2185–2188 (2003).
- ¹⁵G.-T. Ma, J.-S. Wang, and S.-Y. Wang, “Numerical study of the speed-related behavior of the magnetic force in the HTS maglev system based on a 3-d model,” *J. Supercond. Nov. Magn.* **24**, 1593–1598 (2011).
- ¹⁶J. Wang, S. Wang, J. Zheng, F. Yen, G. Ma, L. Liu, J. Li, and W. Liu, “Recent developments of the high temperature superconducting maglev at ASCLab,” *IEEE Trans. Appl. Supercond.* **21**, 1551–1555 (2011).
- ¹⁷Y. Wen, Y. Xin, W. Hong, C. Zhao, and W. Li, “Comparative study between electromagnet and permanent magnet rails for HTS maglev,” *Supercond. Sci. Technol.* **33**, 035011 (2020).
- ¹⁸H. Wang, Z. Deng, S. Ma, R. Sun, H. Li, and J. Li, “Dynamic simulation of the HTS maglev vehicle-bridge coupled system based on levitation force experiment,” *IEEE Trans. Appl. Supercond.* **29**, 1–6 (2019).
- ¹⁹L. Wang, Z. Deng, H. Wang, H. Li, K. Li, and S. Ma, “Dynamic responses of HTS maglev system under track random irregularity,” *IEEE Trans. Appl. Supercond.* **30**, 1–7 (2020).
- ²⁰H. Li, Z. Deng, J. Li, Y. Li, J. Zheng, “Lateral motion stability of high-temperature superconducting maglev systems derived from a nonlinear guidance force hysteretic model,” *Supercond. Sci. Tech.* **31**, 075010 (2018).
- ²¹B. Ren, S. S. Ge, T. H. Lee, and C.-Y. Su, “Adaptive neural control for a class of nonlinear systems with uncertain hysteresis inputs and time-varying state delays,” *IEEE Trans. Neural Netw.* **20**, 1148–1164 (2009).
- ²²X. Zhang, Y. Wang, X. Chen, C.-Y. Su, Z. Li, C. Wang, and Y. Peng, “Decentralized adaptive neural approximated inverse control for a class of large-scale nonlinear hysteretic systems with time delays,” *IEEE Trans. Syst. Man Cybernet. A* **49**, 2424–2437 (2018).
- ²³Z. Liu, G. Lai, Y. Zhang, X. Chen, and C. L. P. Chen, “Adaptive neural control for a class of nonlinear time-varying delay systems with unknown hysteresis,” *IEEE Trans. Neural Netw. Learn.* **25**, 2129–2140 (2014).
- ²⁴Y. A. Kuznetsov, *Elements of Applied Bifurcation Theory* (Springer Science & Business Media, 2013), Vol. 112.
- ²⁵S. Guo and J. Wu, *Bifurcation Theory of Functional Differential Equations* (Springer, 2013), Vol. 10.
- ²⁶S. Guo, Y. Chen, and J. Wu, “Two-parameter bifurcations in a network of two neurons with multiple delays,” *J. Differ. Equations* **244**, 444–486 (2008).
- ²⁷X. Mao and H. Hu, “Stability and Hopf bifurcation of a delayed network of four neurons with a short-cut connection,” *Int. J. Bifurcation Chaos* **18**, 3053–3072 (2008).
- ²⁸P. Bi and S. Ruan, “Bifurcations in delay differential equations and applications to tumor and immune system interaction models,” *SIAM J. Appl. Dyn. Syst.* **12**, 1847–1888 (2013).
- ²⁹K. Engelborghs, T. Luzyanina, and D. Roose, “Numerical bifurcation analysis of delay differential equations using DDE-BIFTOOL,” *ACM T. Math. Software (TOMS)* **28**, 1–21 (2002).
- ³⁰K. Engelborghs, T. Luzyanina, G. Samaey, “DDE-BIFTOOL: A Matlab package for bifurcation analysis of delay differential equations,” *TW Rep.* **305**, 1–36 (2000).
- ³¹J. Sieber, K. Engelborghs, T. Luzyanina, G. Samaey, and D. Roose, “DDE-BIFTOOL v. 3.0 manual-bifurcation analysis of delay differential equations,” *arXiv:1406.7144* (2014).